



OPEN ACCESS

EDITED BY

Maria Chiara Dalconi,
University of Padua, Italy

REVIEWED BY

Manuel Miguel Jordán,
Miguel Hernández University of Elche,
Spain
Virendra Kumar Yadav,
Mody University of Science and
Technology, India

*CORRESPONDENCE

Luciana Mantovani,
✉ luciana.mantovani@unipr.it

RECEIVED 03 March 2023

ACCEPTED 25 April 2023

PUBLISHED 12 May 2023

CITATION

Mantovani L, De Matteis C, Tribaudino M,
Boschetti T, Funari V, Dinelli E, Toller S
and Pelagatti P (2023), Grain size and
mineralogical constraints on leaching in
the bottom ashes from municipal solid
waste incineration: a comparison of five
plants in northern Italy.
Front. Environ. Sci. 11:1179272.
doi: 10.3389/fenvs.2023.1179272

COPYRIGHT

© 2023 Mantovani, De Matteis,
Tribaudino, Boschetti, Funari, Dinelli,
Toller and Pelagatti. This is an open-
access article distributed under the terms
of the [Creative Commons Attribution
License \(CC BY\)](https://creativecommons.org/licenses/by/4.0/). The use, distribution or
reproduction in other forums is
permitted, provided the original author(s)
and the copyright owner(s) are credited
and that the original publication in this
journal is cited, in accordance with
accepted academic practice. No use,
distribution or reproduction is permitted
which does not comply with these terms.

Grain size and mineralogical constraints on leaching in the bottom ashes from municipal solid waste incineration: a comparison of five plants in northern Italy

Luciana Mantovani^{1*}, Chiara De Matteis¹, Mario Tribaudino²,
Tiziano Boschetti¹, Valerio Funari^{3,4}, Enrico Dinelli⁵,
Simone Toller⁵ and Paolo Pelagatti¹

¹Dipartimento di Scienze Chimiche, della Vita e della Sostenibilità Ambientale, Università di Parma, Parma, Italy, ²Dipartimento di Scienze della Terra, Università di Torino, Parma, Italy, ³Consiglio Nazionale delle Ricerche, Istituto di Scienze Marine, ISMAR-CNR Bologna Research Area, Bologna, Italy, ⁴Dipartimento di Biotecnologie Marine, Stazione Zoologica Anton Dohrn, Bologna, Italy, ⁵Dipartimento di Scienze Biologiche, Geologiche e Ambientali, Università di Bologna, Bologna, Italy

Introduction: Bottom ashes (BA) from municipal solid waste incinerators (MSWIs) are currently classified by the European Waste Catalogue as industrial non-hazardous waste. To promote their reuse, identification and characterization of the heavy metal-bearing phases (both glass and minerals), as well as their weathering behavior, must be addressed for what concern the chemical composition, mineralogical phases, and in high concentrations and pollutants' mobility. An important point to be noted is whether the results from a given plant can be generalized.

Materials and methods: In this work, BA from five waste-to-energy (WtE) plants in northern Italy were sorted based on different grain sizes. The area showed similar MSW production, collected from a culturally homogeneous area, and similar collection management. For each grain size, a mineralogical, chemical, and physical characterization was carried out using XRF, XRD, TGA, and the leaching test.

Results and discussion: We found that for major elements, the average chemical composition of the incinerators is similar, with some differences in minor elements. Ferrara (FE) and Forlì-Cesena (FC) BA show portlandite, higher ettringite, and less amorphous than the Torino (TO), Parma (PR), and Piacenza (PC) BA. This affects the pH, the release, and toxicity of the leachates. In FE and FC ashes, ettringite is insoluble, and we not only have low sulfate but also Ni and Ba beyond reglementary limits, suggesting that Ni and Ba are present as hydroxides with portlandite, which are soluble. In TO, PR, and PC, Cr and sulfates are beyond limits, suggesting that Cr comes from dissolution in ettringite. Cu and Cl are always beyond limits; the dissolution of chlorides accounts for only 30%–35% of the global Cl leachate. We observe that in the assessment of the potential toxicity of the ashes, mineralogy has a higher effect than the bulk chemical composition. Grain size sorting, although useful together with other techniques, is not by itself able to comply with the PTE risk level.

Conclusion: The findings contribute to the development of efficient treatment strategies for BA, highlighting the need for a more thorough investigation to understand composition and properties and to find innovative ways to reuse, promoting the circular economy and sustainable waste management practices.

KEYWORDS

municipal solid waste incinerated-bottom ash, potentially toxic element contamination, material characterization, leaching tests, grain size characteristic

1 Introduction

The world generates 2.01 billion tons of municipal solid waste (MSW) per year, of which approximately 33% is not managed in an environmentally safe manner. On average, each individual generates 0.74 kg/day but with strong regional differences. Global waste production is expected to grow up to 3.40 billion tons by 2050 (Kaza et al., 2018).

Waste management in Italy is regulated by the legislative decree no. 152/2006, which implements the main European directives on waste. According to decree no. 152/2006, MSW incineration residues need to be treated before they are disposed of. Landfilling is the most commonly used method to manage MSW, but landfilling also has concerns about groundwater pollution and soil contamination. Among the different waste management options, waste incineration is the most important and widespread option: it reduces the volumes and weight of the waste, and in WtE plants, it also provides a bonus for energy production (Bawab et al., 2021).

Incineration produces two types of solid residues: bottom ashes (BA) and fly ashes (FA). BA are the solid residues resulting from the combustion of household waste at the lower outlet of the furnace, after cooling in the water tank, whereas FA are the blown-out fraction. In general, BA account for approximately 20% of the total waste mass, and FA account for approximately 4% (Izquierdo et al., 2002). FA in Italy are usually excluded from recycling as they contain and release several hazardous elements (Setoodeh Jahromy et al., 2019), while in other countries, they are used in various emerging applications (Yadav et al., 2022).

The BA are composed of mineral fraction (80%–85%), ferrous metals (5%–10%), non-ferrous metals (2%–5%), and unburned organic matter (CEWEP, 2016). The chemical composition of BA depends on the MSW feed characteristics and on the combustion system; the content of major elements resembles on average the content of these elements in the soil and lithosphere. The content of minor and trace elements varies depending on the plant; for most elements, it is depleted, and for some elements, like Zn, Pb, and Cl, it is highly enriched with respect to the equivalent average concentrations found in the soil and lithosphere (Dijkstra et al., 2009). Compared with other combustion waste, BA are highly rich in Cu, Mn, Zn, Pb, Cr, and Ni (Izquierdo et al., 2002). In a circular economy perspective, large quantities of BA can be considered urban mines, from which it could be possible to extract and recycle materials and chemical elements. In this point of view, the chemical and mineralogical characterization of BA is of paramount importance.

In the last 20 years, a number of studies have investigated the technical and environmental properties of BA, and their recycling

methods, leaching behavior, geochemical and petrological aspects. All these literature data stressed the strong complexity of BA due to the intrinsic heterogeneity of the material caused by a) selective collection of household waste, b) choice of incineration technology, c) furnace technology, d) cooling processes, and e) maturation processes (Zevenbergen et al., 1998; Eusden et al., 1999; Meima and Comans, 1999; Piantone et al., 2004; Ginés et al., 2009; del Valle-Zermeño et al., 2017; Dou et al., 2017; Alam et al., 2019, among others).

An important point debated by other authors is the incomplete knowledge of the chemical, physical, and mineralogical composition of the BA, thus making any approach to reuse very approximate (Hyks et al., 2018; Huber et al., 2020).

For example, the finer iron particles mingled within the mineral fraction can hardly be separated by magnets and form several compounds containing heavy metals, which can potentially be recycled (Wei et al., 2011b).

In recent years, much research has been conducted on the use of bottom ashes as concrete in cements (Bawab et al., 2021; Kleib et al., 2021), in ceramic materials (Karamanov et al., 2021; Zanelli et al., 2021), and as fillers in bituminous mixtures (Suárez-Macías et al., 2021). It appears that any such application requires a focus on the chemical and physical features of the bottom ashes, paying attention to their strong heterogeneity and how their mineralogy affects the release of potentially toxic elements (PTEs) in the environment.

The characterization of waste from incinerators in terms of chemical and mineralogical variation is preliminary to possible reuse paths. A critical parameter was found to be grain size. It was shown that chemical composition changes with grain size and that several PTEs are concentrated in the finer fractions (Chimenos et al., 1999; Wei et al., 2011a; del Valle-Zermeño et al., 2017; Šyc et al., 2018; 2020). More recent investigations, however, contend with the aforementioned scenario as a general rule, showing for a given element differences in grain size vs. composition in different incinerators (Caviglia et al., 2019; Loginova et al., 2019; Huber et al., 2020; Mantovani et al., 2021). A limitation to the aforementioned investigations is the lack of data on a quantitative mineralogical composition that changes with grain size, together with leaching tests, to determine the possible release of PTEs.

In this work, the chemical, physical, and mineralogical analysis of BA from five plants located in northern Italy has been carried out. The areas show similar MSW production, collected from a culturally homogeneous area, and similar collection management. This will reduce the bias for possible differences in the input, which affect such comparisons between incinerators. The samples were sorted according to the particle size and then analyzed to understand the variability arising from this parameter. XRD, XRF, and TGA were

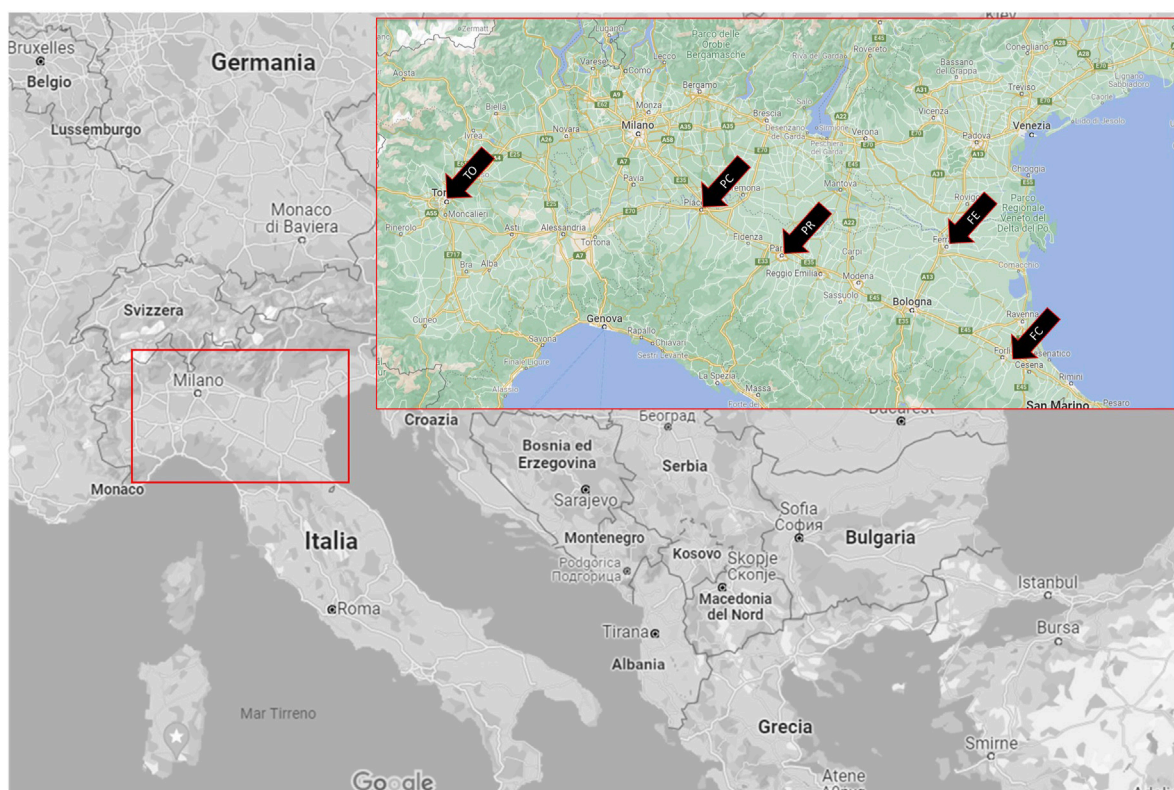


FIGURE 1
Geographical distribution of WtE plants investigated in this work.

performed on each portion, followed by leaching tests. Grain size, elemental composition, and leachate products were studied by principal component analysis (PCA).

This work aims a) to describe the mineralogical and chemical variability between the bottom ashes from different WtE facilities, arising from plant performance during incineration and weathering; b) to provide general relationships between grain size and composition and between the different elements, for bulk and leachates, in order to assess the potential of grain size sorting for a higher value use of the ashes; and c) to provide new suggestions to foresee potential leaching from the mineralogical composition of the ashes.

2 Materials and methods

2.1 MSWI bottom ash sampling and sorting

The samples were collected from five WtE plants located in northern Italy, three of them owned by *Iren Ambiente 2018 S.p.A* (Parma, Torino, and Piacenza, hereafter PR, TO, and PC) and two by *Herambiente S.p.A* (Ferrara and Forlì-Cesena, hereafter FE and FC) (Figure 1). Table 1 summarizes for each plant the starting date of the activity, the type of waste input (tons/year), and the total weight of BA produced. All the plants analyzed use grate furnace technology that burns the waste for 2 to 3 hours at temperatures between 750°C and 1,000°C. The input waste includes approximately 80% of the

undifferentiated fraction of separate collection (approximately 80%) and approximately 20% of special non-hazardous waste (industrial and household waste, sewage sludge, cemetery waste, and biomedical waste). Only MSWI is burned in the Forlì plant (*Iren Ambiente S.p.A.*, 2018; *Herambiente S.p.A.*, 2020). The BA sampling from the plants was carried out during a typical day of the process activity in different periods, as reported in Table 1. Samples were randomly taken from a 2–3-m-high stockpile, which is representative of more than 1 month of accumulation. The homogeneity was checked by making X-ray diffractions on repeated days, without showing any significant difference. The samples were taken in May 2019 in PR, TO, and PC WtE plants and in April 2020, during the pandemic lockdown, in FE and FC. Approximately 5 kg of BA samples were collected from each plant. Before the analysis, the ashes were mixed, dried in an oven at 50°C for 24 h, and sieved to isolate different size classes. The sequential sieving (Φ : 16, 8, 4, 2, 1, 0.5, 0.3, 0.2, and 0.63 mm) was performed according to the European standards for aggregates EN 933–2 (*Ente Nazionale Italiano di Unificazione*, 2020). The cumulative grain size distribution curves are shown in Figure 2. Aggregates larger than 3 cm were removed to avoid loss of representativeness and distortion of the analytical results.

2.2 XRD analysis

X-ray powder diffraction (XRD) was performed on each sieved fraction. A Bruker D2 Phaser powder diffractometer was used,

TABLE 1 Waste input and output (only for BA) for each sampled WtE plant. Municipal solid waste: household and similar waste; special waste: waste from municipal sewage network and treatment, municipal construction and demolition waste, and sanitary and cemetery wastes (data from: [Iren Ambiente, 2018](#); [Hera Ambiente, 2020](#)).

WtE plant	Operating since (using this setup)	Waste input (tons/y)	% of the waste type	Total waste input	BA produced (tons/y)	Data related to	Sampling date for this work
Parma	2014	Undifferentiated municipal solid waste (MSW)	126317	79	159 832	32 904	2019
		Special wastes (SW)	33515	21			
Piacenza	2002	Undifferentiated municipal solid waste (MSW)	110041	96	114 231	21 135	2018
		Special wastes (SW)	4190	4			
Torino	2014	Undifferentiated municipal solid waste (MSW)	457603	81	562 269	118 969	2019
		Special wastes (SW)	104666	19			
Ferrara	2008	Undifferentiated municipal solid waste (MSW)	69598	53	131 894	27 021	2020
		Special wastes (SW)	62296	47			
Forli	2008	Undifferentiated municipal solid waste (MSW)	119215	100	119 215	53 308	2020

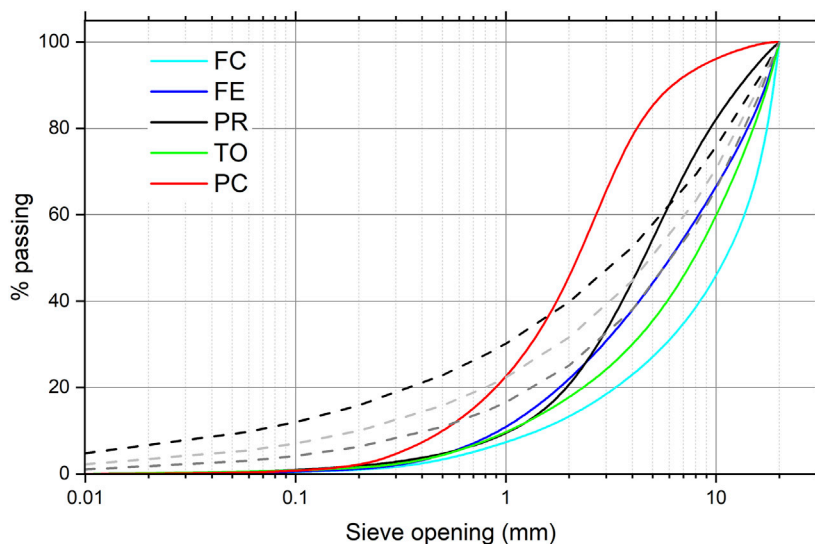


FIGURE 2

Cumulative particle size distribution of bottom ashes of the five plants analyzed. The dashed lines represent the Fuller's curves with $n = 0.4, 0.5,$ and 0.6 and $d_{max} = 20$ (Fuller and Thompson, 1907).

operating at 30 kV and 10 mA with $\text{Cu K}\alpha$ ($\lambda = 1.54178 \text{ \AA}$) radiation. The collections were carried out at 2θ between 5 and 100° , steps of 0.02° , and 1 s/step sampling time. The diffractometer works with θ - θ focalizing geometry and takes an advantage of a solid-state detector. A 30 rpm sample rotation was applied to minimize crystal

preferential orientation effects. The diffraction patterns were identified using the Bruker software EVA and the Crystallography Open Database (COD) (Table 2). The GSAS 2 software package (Toby and von Dreele, 2013) was used to perform Rietveld analysis and quantify the major crystalline

TABLE 2 XRPD identification of bottom ashes. The minerals are arranged in the following sequence: (x) major minerals, (*) minor, or trace minerals (/) not found or very doubtful presence.

Mineral phases		WtE plant				
Name	Formula	PR	PC	TO	FE	FC
Calcite	CaCO ₃	x	x	x	x	x
Vaterite	CaCO ₃	x	x	x	x	x
Quartz	SiO ₂	x	x	x	x	x
Cristobalite	SiO ₂	/	/	*	/	/
Anorthite	Ca(Al ₂ Si ₂ O ₈)	x	x	x	x	x
Bytownite	(Ca,Na)[Al(Al,Si)Si ₂ O ₈]	x	x	x	x	*
Albite	Na(AlSi ₃ O ₈)	*	*	*	/	/
Pyroxene group	ABSi ₂ O ₆	/	/	x	/	/
Akermanite	Ca ₂ Mg(Si ₂ O ₇)	*	*	*	x	x
Gehlenite	Ca ₂ Al(AlSiO ₇)	x	x	x	*	*
Ettringite	Ca ₆ Al ₂ (SO ₄) ₃ (OH) ₁₂ · 26H ₂ O	x	x	x	x	x
Hydrocalumite	Ca ₄ Al ₂ (OH) ₁₂ (Cl,CO ₃ ,OH) ₂ · 4H ₂ O	x	x	x	x	x
Portlandite	Ca(OH) ₂	x	x	x	x	x
Strätlingite	Ca ₂ Al ₂ SiO ₇ · 8H ₂ O	x	/	/	/	/
Apatite	Ca ₅ (PO ₄) ₃ (Cl/F/OH)	*	*	*	*	*
Larnite	Ca ₂ SiO ₄	*	*	*	x	x
Tobermorite	Ca ₄ Si ₆ O ₁₇ (H ₂ O) ₂ · (Ca · 3H ₂ O)	*	*	*	/	/
Sjogrenite	Mg ₆ Fe ₂ (OH) ₁₆ (CO ₃) · 4H ₂ O	/	/	/	*	*
Magnetite	FeFe ₂ O ₄	x	x	x	x	x
Ematite	Fe ₂ O ₃	x	x	x	x	x

phases and the amorphous content. High-purity Al₂O₃ corundum (10 wt%) was used as an internal standard. [Supplementary Table S1](#) reports the quantitative interpretation of XRD analysis with grain size for each WtE plant.

2.3 XRF analysis

The bulk composition of each grain size was measured using a Analytical Axios 4000 wavelength dispersive X-ray fluorescence (XRF) spectrometer, equipped with an Rh tube. Approximately 3 g of the representative samples were oven-dried at 50°C, homogenized, and milled using an agate vibratory disk mill. Thin-layer pressed powder pellets for XRF analysis were prepared using a boric acid binder. The reproducibility, the general accuracy via a calibration curve, and corrections of the data followed the same methods similar to those used in other works ([Franzini et al., 1972](#); [Toller et al., 2021](#)). Major, minor, and trace element (SiO₂, TiO₂, Al₂O₃, Fe₂O₃, MnO, MgO, CaO, Na₂O, K₂O, P₂O₅, As, Ba, Br, Ce, Cl, Co, Cr, Cu, Ga, Hf, La, Mo, Nb, Ni, Pb, Rb, S, Sc, Sn, Sr, Th, U, V, W, Y, Zn, and Zr) concentrations were calculated using a calibration curve built on a large number of certified reference materials and offline

correction of loss-on-ignition (LOI) values. The LOI, which is correlated with the influence of humidity, organic matter, and water, was gravimetrically estimated after heating the samples overnight at 950°C in a muffle furnace ([Heiri et al., 2001](#)).

2.4 TGA

Thermal gravimetric analyses (TGA) were conducted using a PerkinElmer 8000 instrument equipped with a Pt crucible (sample mass approximately 3–5 mg) at a heating rate of 10°C/min in the temperature range of 35°C–800°C. All the measurements were run under a constant flux of dry air (30 mL/min).

2.5 Leaching tests and water elemental analysis

Standard leaching tests and analysis of the leachates were performed following the European normative (adopted in Italy) EN 12457-2 (2004) on Waste Characterization–Leaching–Compliance Test for Leaching of Granular and Sludge Waste ([EN, 2004](#)).

The EN test is based on a one-stage batch at a defined liquid-to-solid ratio (L:S = 10:1) for materials with particle sizes below 4 mm that can or cannot be ground. In this work, the tests were carried out on the five smaller grain sizes: 0.063–0.2, 0.2–0.3, 0.3–0.5, 0.5–1, and 1–2 mm for all the five WtE plants examined. Three replicates of 30 mL: 3 g of samples were prepared for each class portion to minimize the variability of the samples, together with a “blank” containing only 30 mL of ultrapure water. Samples and ultrapure water (Milli-Q[®] 18.2 MΩ cm at 25°C and TOC <5 ppb) were put in hermetically sealed bottles for 24 h in a shaking device (30 rpm) and in a controlled environment. Then, the solid fraction and the eluates were separated with 0.45-μm membrane filters using a vacuum filtration device, and the pH and temperature of the solutions were measured. The analysis of the leachate samples was conducted by ion chromatography (Metrohm Compact IC Pro 881) for anions (Cl⁻, SO₄⁻², F⁻, Br⁻, and PO₄³⁻), atomic absorption spectroscopy (Thermo S Series AA Spectrometer) for cations (Ca, Mg, Na, and K), and inductively coupled plasma mass spectrometry (PerkinElmer ICP-MS ELAN DRC-e) for trace elements (Al, Ba, B, Cr, Co, Fe, Pb, Li, Mn, Mo, Ni, Se, Sr, Tl, Ti, V, and Zn). Generally, the detection limit of the analytical techniques used was below 0.01 ppb for the majority of elements, even lower for Cd, Cu, Co, Mn, Mo, and Pb (up to 0.005 ppb), and slightly higher for halogens (approximately 10 ppb). The relative standard deviations for most elements in the leaching experiments were within 10%.

Finally, the metal extraction (from the solid to the leachate) was calculated using the following formula: $X_{\text{lea}}/X_{\text{bulk}} \cdot 100$ for each WtE plant with a grain size <2 mm, where X_{lea} is the analytical determination of a certain element in the leachate and X_{bulk} is the total concentration of the solid by XRF.

3 Results and discussion

3.1 Particle size distribution

Figure 2 shows the grain size distribution curves of the samples. In all the BA samples, the larger fraction prevails: below 1 mm, the sieved portion represents between 5 and 8 wt% of the total mass, and 50% of the mass does not pass the 4 mm sieve. This was also found in previous investigations (del Valle-Zermeño et al., 2017; Šyc et al., 2018; Caviglia et al., 2019). An exception is the PC plant, where there is a higher percentage of fine and medium-sized particles (the grain passage is almost 80% at 4 mm). It is not clear whether this is due to the sampling methodology or the intrinsic heterogeneity of MSWI residues. To test the recyclability of BA in cementitious formulations, we compared our results with the optimum size distribution for concrete according to Fuller's curve, which represents the optimal aggregate distribution curve in terms of density and strength (Fuller and Thompson, 1907). The optimum percentage of a given particle diameter d is calculated by Fuller's curve using the following formula: $p(d) = 100(d/d_{\text{max}})^n$. Three Fuller's curves were calculated with an aggregate maximum value of $d_{\text{max}} = 20$ mm, i.e., the maximum opening sieves used here, and an exponential factor $n = 0.4, 0.5,$ and 0.6 . In no case, the distribution falls completely within the curves, as the smaller dimensions are underrepresented in our sampling.

3.2 XRD

Table 2 and Supplementary Table S1 show the mineralogical composition of the BA and their separated grain size classes. The bulk mineralogical composition of the ashes for each incinerator was obtained from that of each grain size and their proportion as follows:

$$c_{i,\text{bulk}} = c_{ij} \cdot w_j / w_{\text{bulk}},$$

where $c_{i,j}$ is the fraction of the mineral (i) in the sieved portion (j) (as reported in Supplementary Table S1), w_j is the weight of the sieved portion, and w_{bulk} is the weight of the sum of the sieved portions.

The minerals reported in Supplementary Table S1 are those present abundantly, whose abundance could be refined by Rietveld analysis. A number of minor phases is also present, which either showed very faint peaks in XRD or could be detected just from microprobe analysis (Bayuseno and Schmahl, 2010; Mantovani et al., 2021). During Rietveld analysis, it was shown that the inclusion of a higher number of phases leads to refinement instability so that a compromise was necessary between the number of phases to be included and the number of phases that could be refined. In some cases, the identification of mineral phases was doubtful due to the overlap of identificative reflections associated with certain peaks (Table 2).

Most evident is the amorphous content, which is higher in the BA of the three plants (TO, PR, and PC) so that it overtakes the entire quantitative of crystalline component. In these plants, the amorphous content is over 75% on average, and the grain size ranges between 67 and 88 wt%. In FE and FC plants, instead, bulk amorphous is, on average, less than 35% (depending on grain size between 7 and 55 wt %). Furthermore, there is a slight inverse correlation between the logarithm of the grain size and the amorphous content, with $R^2 = 0.64, 0.53,$ and $0.41,$ for PR, PC, and TO, respectively. For FE and FC, the correlation is not significant ($p > 0.05$) (for statistical value, see Supplementary Table S4).

A large amount of amorphous material is common in bottom ashes (Eusden et al., 1999; Bayuseno and Schmahl, 2010; Caviglia et al., 2019; Loginova et al., 2019; Šyc et al., 2020, among others). More recently, Mantovani et al. (2021) showed that several amorphous phases characterized by different compositions, formation, and likely micro-structure are present rather than a single homogeneous amorphous phase. Residual glasses collected from the input waste are mostly present in the larger grains, whereas in fine grains and in some areas of aggregates, partly melted glasses are also present. Microprobe analyses on this glass portion showed that they have different compositions; in general, they coexist with crystals under eutectoid conditions, with the local composition depending on the metal (transition, alkali, and alkali earth) content.

The lower quantity of amorphous material in FE and FC occurs together with higher content of calcite, quartz, and feldspar. Furthermore, ettringite content is higher in FE and FC than in the other three plants sampled, indicating a probable greater reactivity of these ashes in the aging process. FE and FC showed the presence of larnite and portlandite, probably due to the high Ca content and ascribable to the carbonation reaction and cementitious material in the input feed.

Among minerals, quartz, calcite, melilites, iron oxides, and some alteration products such as sulfates, chlorides, and hydrated minerals are ubiquitous. An inverse relationship with grain size is found in calcite, mainly in TO and PR incinerators ($R^2 = 0.95$ and

0.82, respectively) and less in PC and FC (0.53 and 0.45). In FE bottom ashes, the relationship is not significant, but the larger size shows a much lower calcite content than the finer portion. Calcite is probably derived from secondary carbonation, during weathering in the temporary storage site, but we do not exclude the possibility that the higher calcite content in FE and FC may come from an unfinished de-carbonation process during thermal decomposition. Portlandite, $\text{Ca}(\text{OH})_2$, is found only in the BA ashes from FE and FC as a product of rehydration of CaO. The Ca-oxide forms from the de-carbonation reaction at approximately 700°C and an initial atmospheric partial pressure (0.04 atm) (Criado et al., 2018):



In FC, portlandite correlates with the amorphous content ($R^2 = 0.72$). Such a positive correlation is also found, albeit portlandite correlates with lower amorphous content, evidenced in Ferrara ($R^2 = 0.34$).

Ettringite, hydrocalumite, and strätlingite are formed during weathering. Ettringite and hydrocalumite are ubiquitous, whereas strätlingite is found only in the PR plant. Ettringite in TO is positively related to calcite and hydrocalumite ($R^2 = 0.82$ and 0.83 , respectively) and shows a negative correlation with grain size ($R^2 = 0.78$). A milder correlation is found between ettringite and grain size in PR and FE, whereas in FC, no correlation is found. In PC, ettringite shows an inverse correlation with calcite, and calcite has a positive correlation with hydrocalumite.

Strätlingite is found only in the PR samples. This mineral is typical of cementitious materials and can be formed either from the degradation of gehlenite or from the reaction between calcium silicates (Ca_2SiO_4 , belite), with $\text{Al}(\text{OH})_3$ in hydration processes (Winnefeld and Lothenbach, 2010; Rungchet et al., 2017). In this case, the formation of strätlingite does not involve the degradation of gehlenite, as some evidence found in SEM analyses and reported in a previous work (Mantovani et al., 2021) showing that gehlenite has been formed in the combustion chamber (crystals with typical neoformation and rapid cooling shape).

Another cement-related phase, larnite, is present in significant amounts in FE and FC. It is found at higher values in the smaller size fraction. A doubtful identification of tobermorite in PR, PC, and TO would indicate that C-S-H formation has occurred.

Iron-containing minerals such as hematite and magnetite are revealed by X-ray diffraction, although other metal phases are likely present like Cu or Ni-Ti alloys, as reported by Mantovani et al. (2021).

Lastly, a number of silicate phases, such as pyroxene, gehlenite-akermanite, and anorthite, are found without significant differences in grain size and are likely formed at high temperatures in the combustion chamber.

3.3 XRF

As already observed by numerous authors, the bulk chemical composition of BA is represented by the major oxides of Si, Ca, Fe, and Al (Supplementary Table S2) (Bayuseno and Schmahl, 2010; Funari et al., 2015; Caviglia et al., 2019, among others). In fact, the sum of these elements (in oxides) represents from 60 to 77 g/100 g. S and Cl are found in a range of 0.3–2 g/100 g. Among minor elements, the content of Zn, Cu, Pb, and Ba is higher than 1,000 mg/kg. Supplementary Table S2 presents the content of

major, minor, and trace elements divided by grain size for all the investigated plants. Figure 3 represents the value range (max and min) for each element and plant, with a comparison of the range of the average composition of the incinerator value reported by Astrup et al. (2016). The compositional variability of the major elements shown by different grain size portions in the five incinerators is rather close, when compared to the variability reported by Astrup et al. (2016). The similarity between the bottom ashes from the plants investigated in this work is confirmed by comparing the weighted average composition. In Figure 4A, the oxides show a rather similar pattern in different plants, albeit some slight differences exist: the BA from TO show higher Fe_2O_3 and lower CaO, and those from Piacenza show lower SiO_2 and higher LOI than the others. Furthermore, for minor elements, our data show that the compositional variability related to grain size is small compared with the variability shown by Astrup et al. (2016). However, the difference in the average composition between the BA from different plants is more marked. In Piacenza higher values are found for Cl and Cu, and overall, there is a higher compositional spread in S, Cl, and Zn content (Figure 4B). The analysis of the relationship of composition with grain size and between elements in the different grain size portions was carried out by bivariate analysis and PCA (Supplementary Figure S1).

Bivariate analysis (Supplementary Table S4) shows that Si positively correlates with grain size ($p < 0.05$), probably due to the glass shards in larger grain size. Na also correlates with Si, possibly due to the addition of Na as a fining agent in glass production technology and the presence of plagioclase solid solution. Ca, Ti, S, loss on ignition (in all the plants), and Cl (in PR, PC, and FE) correlate negatively with grain size. The smaller fraction is richer in Ca due to the faster carbonation occurring in smaller particles with a larger surface area. The higher Ca content in smaller particles goes along with the higher Ca-carbonate content. Higher de-carbonation also means higher weight loss in LOI, which is greater in smaller particle sizes with higher active surfaces. We suppose that S follows the same trend due to the sulfation process and the formation of the ettringite phase, which, as shown in XRD analysis, is present more in finer-sized grains. Most of the PTEs like Cu, Pb, and Cr are negatively related to grain size. Of note, the differences in the concentration of minor elements between plants are within an order of magnitude and could be related to the different waste inputs. Other elements, like Al, Fe, Mg, P, and Cr, show little change between samples of different grain sizes. An exception is observed in Torino MgO and Al_2O_3 , which shows a significant increase in the smaller-sized grains.

S and Cl (Figure 5) are present in the BA in considerable quantities, causing metal erosion if they are used as supplementary cementitious material in reinforced concrete (Ito et al., 2006). In BA examined in this work, S and Cl range between 2,000 and 21,000 mg/kg. These two elements are positively correlated in all incinerators and show an inverse correlation with the grain size, as already pointed out by Alam et al. (2020), suggesting that they are mostly present as weathering of the products.

Principal component analysis (Supplementary Figure S1) was carried out to study the element composition and grain size of the BA from each incinerator and to seek the variability and trends for each element.

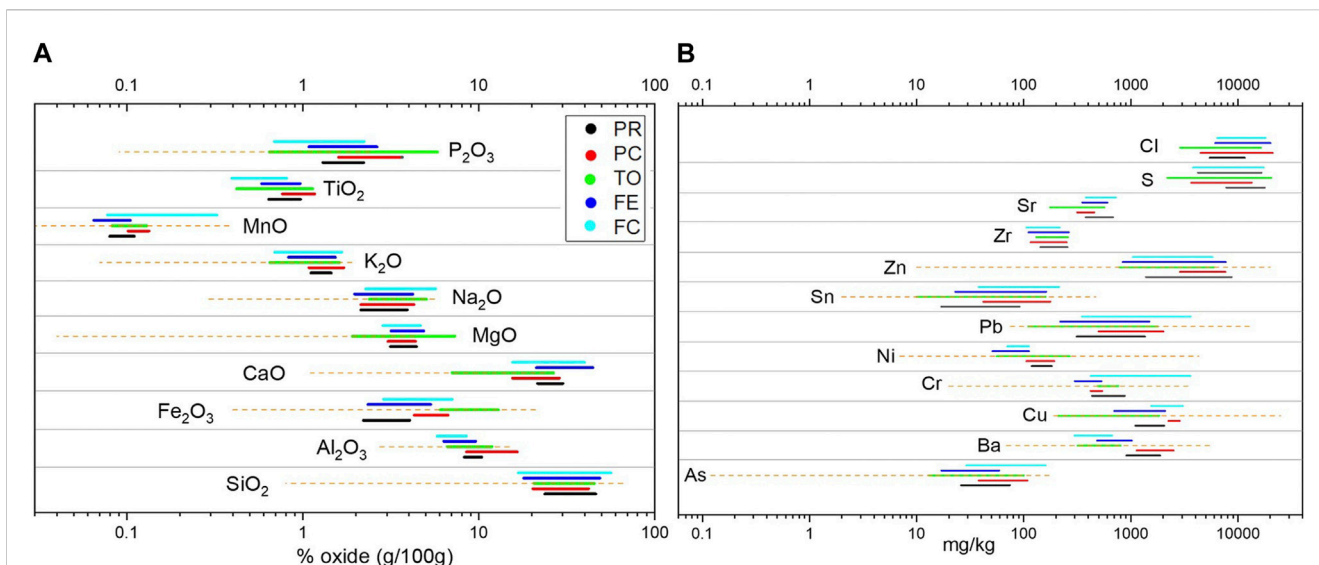


FIGURE 3
Ranges observed for (A) major (g/100 g in oxides) and (B) minor (mg/kg in elements) element content of BA from the five WtE plants (different color) examined. Orange dot lines represent the minimum-to-maximum range found in several literature sources and reported by Astrup et al. (2016).

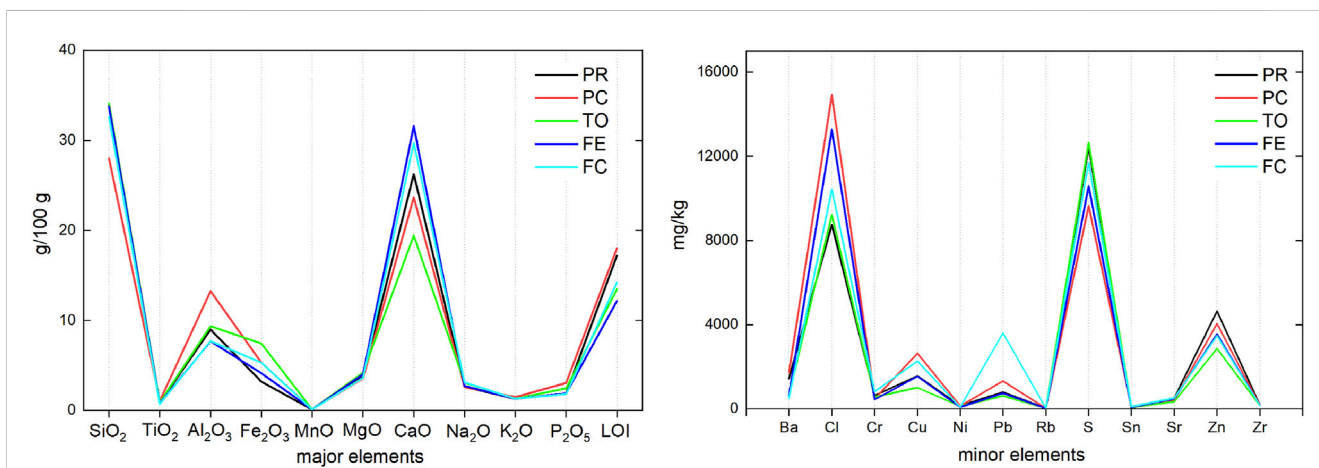


FIGURE 4
Weighted average composition of the major (g/100 g in oxides) and minor (mg/kg in elements) elements for each WtE plant analyzed.

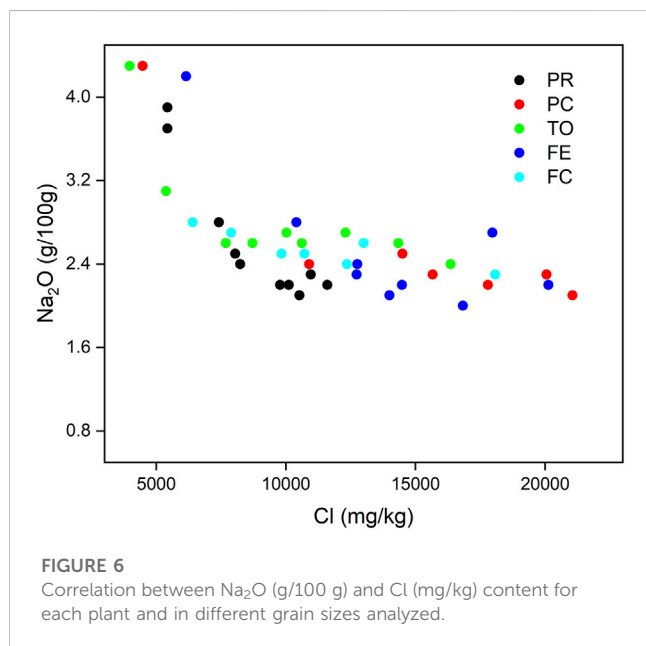
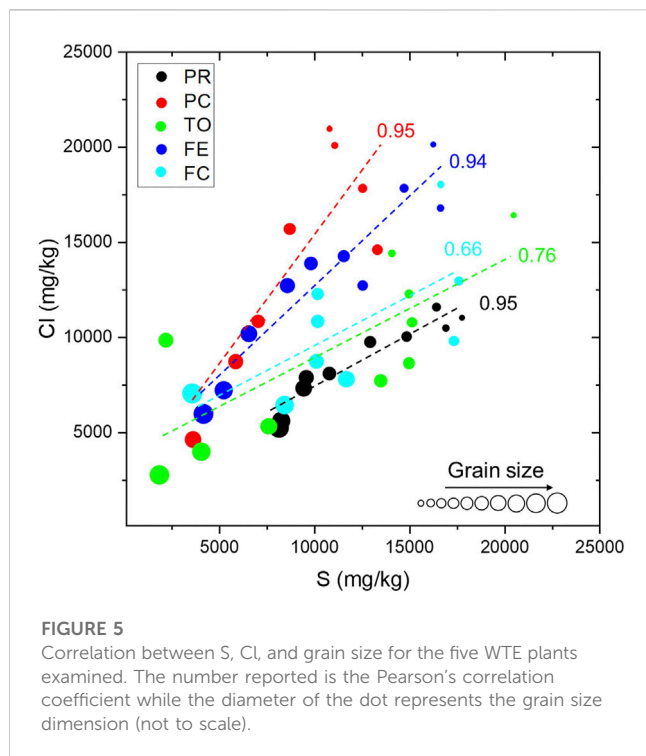
In the analysis of previous data on the Parma WtE plant, Mantovani et al. (2021) found a relationship between CaO, LOI, S, and Cl, which have an opposite variation with SiO₂, grain size, and lithophile elements like Zr and Rb. This is also confirmed by PCA of other incinerators, with Zn and Sn that, with the exception of Piacenza, follow the LOI and S. Ni, Cr, and Pb do not follow one of the two trends and do not show a definite grouping with other PTEs. In Piacenza and Ferrara, Ni and Cr are oppositely related to the second component; Pb is also unrelated with the aforementioned elements, with the exception of Ferrara, where it correlates with S and a possible grouping with As. More complex, non-linear relationships are also observed.

For instance, Na₂O in the larger grains is negatively related to Cl, whereas when Cl exceeds 5,000 mg/kg, Na₂O does not change with the increase in Cl. Higher Na content is locked in the glass and high-

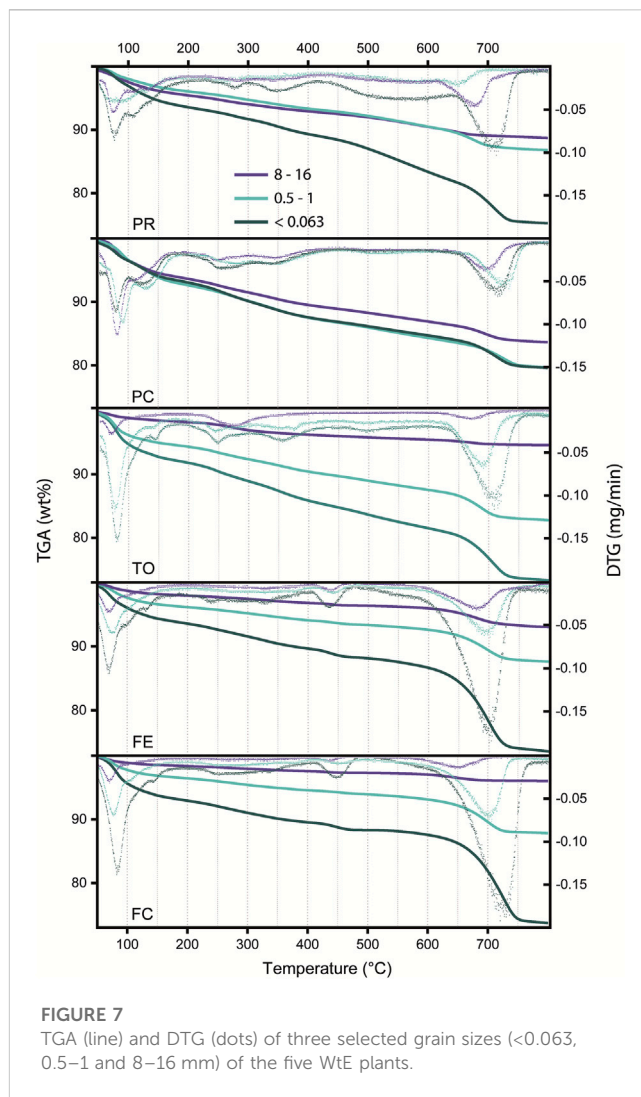
temperature minerals in the larger grains, whereas in the smaller ones, Na becomes more linked to Cl in chlorides, probably due to the decomposition of the glasses by weathering (Figure 6). This will be confirmed by further analysis of the leachates.

3.4 Thermogravimetric analyses

Thermogravimetric analysis shows a continuous weight decrease with temperature for any grain size. The weight loss is higher in the smaller grain sizes, where the mass loss at 800°C is approximately 25%. For the larger grain size, the loss is about 5%–10%, and for the intermediate ones, it is approximately 15%. An exception is PC, where the weight loss is similar for every grain size (Figure 7).



The analysis of the first derivative shows few temperature ranges where higher weight loss is present. A moderate (3%–4%) weight loss occurs in the interval 50°C–100°C, which is likely ascribed to two reactions: one at 50°–60°, likely due to surface water, and another just above 100°C, related to the first dehydration of ettringite, with further dehydration possibly revealed by the faint peaks at 250°C and 350°C (Fridrichová et al., 2016).



The second loss is in the range of 1–2 wt% and appeared over the range 250°C–450°C and a 4–7 wt% in the interval 620°C–760°C. The 250°C–450°C reaction is likely due to plastic combustion residue (molecular decomposition), as suggested by Trifunovic et al. (2010), while the 620°C–760°C loss is ascribable to the transformations involving carbonate (de-carbonation) phases. The first mass loss at approximately 100°C can be related to surface water.

In FE and FC, the de-carbonation loss is greater than that in the other plants, which is consistent with XRD and XRF data that show a higher carbonate content.

Despite the general shape of the TGA curves appearing similar, some differences in particle size dimensions and between plants are found. A peak at 450°C has been found only in FE and FC BA. The peak is more apparent in the finer portion, and it is likely due to the dehydration of portlandite (Menéndez et al., 2012), which occurs between 450°C and 500°C. Portlandite is present only in the two incinerators of FE and FC, between 5 and 10 wt% in the finer portion and between 1% and 2% in the larger grains.

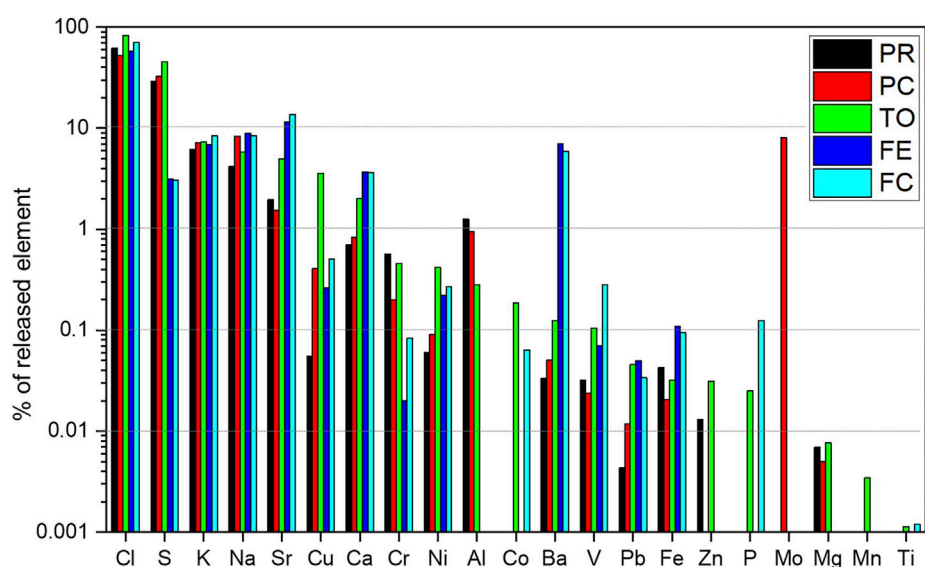


FIGURE 8
Percentage of released elements calculated using $(X_{\text{bulk}}/X_{\text{lea}}) \cdot 100$ for each WtE plant in the grain size <2 mm.

3.5 Leaching tests

Leaching tests were carried out on particles of sizes below 2 mm, as XRF analyses showed that they are richer in PTE. The leaching was performed on particles of different sizes, and their variability was analyzed by PCA. The results are reported in [Supplementary Figure S2](#) and [Supplementary Table S3](#).

PCA analysis shows that the two major components describe more than 80% of the variability in all WtE plants. A number of ions, such as Cl, K, Li, Na, and Cu, show an opposite trend with respect to grain size, i.e., show higher leaching in smaller-sized samples. SO_4^{2-} follows Cl in TO, PR, PC, and FC. In FE and FC, the sulfates leached are one order of magnitude less than those in other incinerators. Ni and Cr follow Cl and sulfates in TO, PR, and PC, but not in FE and FC. Pb does not follow a definite trend, with little change in grain size. Al is leached in significant amounts only in TO, PR, and PC, but not in FE and FC.

Marked differences in leaching behavior have been found between the two different owner corporations: IREN for PR, PC, and TO and HERA for FC and FE.

Although the leaching is generally higher in the smaller grain size portion, a great difference, within one order of magnitude, is found. Higher differences are observed between WtE plants.

With respect to a given particle size, the leaching of an element has been compared to the total content in the bulk sample (from XRF analysis) and calculated in percentage (all referred to as mg/kg of material). The most released element is Cl, with a release percentage of about 70–90%, which is higher in the finer fraction ([Figure 8](#); [Figure 9](#), [Supplementary Table S3](#)). The extraction efficiency in the smaller portion is almost twice compared to that in the larger portion. In agreement with [Alam et al. \(2020\)](#), we suggest that Cl is present in highly soluble salts, such as NaCl and KCl, dispersed on the surface of the grains. This suggestion is confirmed by the linear relationship found in leached Na + K

with Cl ([Figure 9A](#)), whereas such a relationship does not exist in the sample composition determined by XRF as most Na and K are likely caged within the amorphous and silicate structures. However, the amount of chlorides in leachate is considerably greater than the Na + K value (and not in a 1:1 ratio), suggesting that the release of Cl is not only attributed to the dissolution of the Na/K salts. Therefore, no diffraction peaks attributable to Na and KCl are found in XRD analysis, suggesting that not all Cl is bound to Na and K in salts and that a significant release of Cl may originate from the dissolution of ettringite.

Therefore, the contribution of ettringite dissolution is probably minor, due to the very similar ratio in Na + K/Cl in the five plants, in spite of different amounts and solubilizations of ettringite ([Figure 10](#)).

EDS analyses of the ashes from PR ([Mantovani et al., 2021](#)) showed that Cl is often associated with silicate glassy phases. We suggest therefore that chloride is mostly released by the dissolution of weakly bonded Cl at the surface of the amorphous phases. This would explain the higher leaching in smaller grains with a higher surface.

All tests exceeded the legal limits for Cl (Legislative Decree 152/06), suggesting that washing and selection of larger grains may be combined to reduce Cl for correct reuse.

S shows a release, approximately 30% for PR, PC, and TO and 3% for FE and FC, with no dependence on the particle size. S is present in the ettringite structure, which is observed in XRD in all the plants, especially in FE and FC. However, the release of SO_4^{2-} is lower in the two HERA WtE plants, whereas Ca is higher ([Figure 9B](#)). Moreover, Al is released by at least two orders of magnitude less in HERA than in IREN plants. Another relevant difference is that the measured pH in the leached IREN plants is between 10 and 11, whereas in the HERA plants, it varies between 12 and 12.5. We suggest that in the HERA plants, the dissolution of portlandite, which is absent in the IREN plants, gives rise to a basic

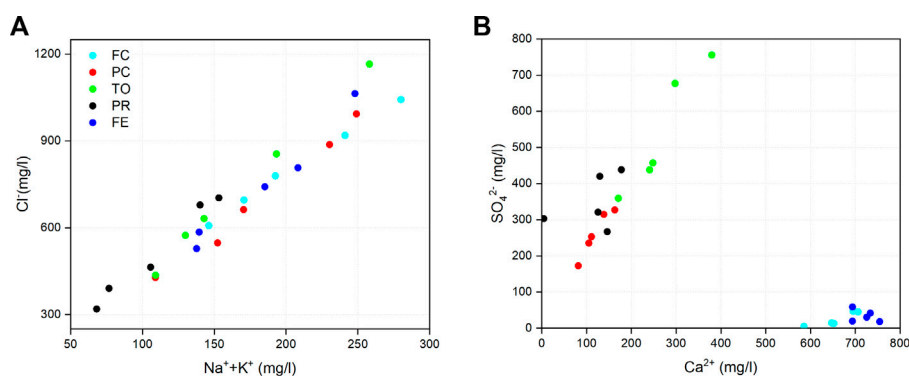


FIGURE 9 Correlation between the leached $\text{Na}^+ + \text{K}^+$ vs. Cl^- and SO_4^{2-} vs. Ca^{2+} (mg/L).

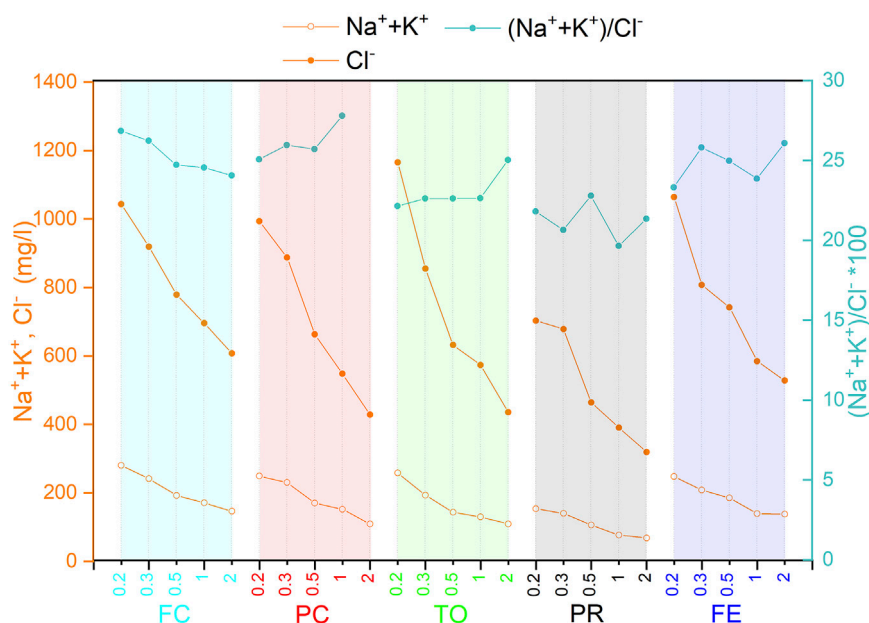


FIGURE 10 Trend of $\text{Na}^+ + \text{K}^+$, Cl^- , and $\text{Na} + \text{K}/\text{Cl}$ in the leachate depending on the grain size (<2 mm) for the five WtE plants.

environment, where ettringite is less prone to dissolution. In the IREN plants, ettringite dissolves with sulfate and Al hydroxide solubilization.

Other elements like Mg and Fe do not show significant leaching, indicating that they are bonded in non-soluble oxide or silicate structures.

The different mineralogy in IREN and HERA plants and the consequent different leaching of major elements also have an effect on minor elements. Minor elements are often present in solid solutions within phases more or less prone to dissolution at different pH, and the dissolution of the host phases also releases the exsolved element. Therefore, the release of minor elements is

different in the different WtE plants, often by two orders of magnitude. In some plants, the leaching could be above legal limits, whereas in others it could not (Table 3). For instance, sulfate and Cr are above regulatory limits only in IREN BA, but Ba and Ni (with the exception of TO) are above regulatory limits only in the HERA plants. Sr leaching is observed in high percentages in FE and FC (10%–15% of the bulk) and less in the IREN plants (4%–6% in TO and 1%–2% in PR and PC). A likely interpretation is that Cr could have a significant concentration in ettringite, which is dissolved in IREN plants, whereas Ba, Ni, and Sr could exchange with Ca in a significant amount in portlandite, which is dissolved in HERA plants.

TABLE 3 Leaching test results for elements subject to regulation for plants (d.lgs 156/2006). Red indicates concentrations exceeding legal limits.

Element		Cl ⁻	SO ₄ ²⁻	F ⁻	PO ₄ ³⁻	Ba	Cu	Zn	As	Be	Co	Ni	V	Cd	Cr	Pb	Se
Legal limit		100 mg/l	250 mg/l	1.5 mg/l	2 mg/l	1 mg/l	0.05 mg/l	3 mg/l	50 ug/l	10 ug/l	250 ug/l	10 ug/l	250 ug/l	5 ug/l	50 ug/l	50 ug/l	10 ug/l
WtE plant	Grain size (mm)	mg/l							ug/l								
		PR	0.063–0.2	703	438	0	0	0.04	0.12	0.06	0	0	0	8	2	0	458
PR	0.2–0.3	678	420	0	0	0.04	0.09	0.06	0	0	0	8	2	0	354	0	17
PR	0.3–0.5	463	321	0	0	0.04	0.07	0.06	0	0	0	7	2	0	248	2	13
PR	0.5–1	391	267	0	0	0.05	0.05	0.04	0	0	0	8	2	0	212	4	19
PR	1–2	319	303	1.0	0	0.04	0.04	0.05	0	0	0	4	2	0	198	2	8
PC	0.063–0.2	993	327	4.5	0	0.08	1.15	0	0	0	0	4	2	0	119	4	62
PC	0.2–0.3	887	315	0	0	0.06	1.17	0	0	0	0	2	2	0	105	2	56
PC	0.3–0.5	662	253	11.4	0	0.06	0.88	0	0	0	0	2	2	0	74	2	46
PC	0.5–1	547	236	3.0	8	0.08	0.95	0	0	0	0	38	2	0	75	59	32
PC	1–2	428	173	3.9	0	0.04	0.36	0	0	0	0	0	0	0	31	0	34
TO	0.063–0.2	1,170	756	0	0	0.09	5.31	0.11	0	0	11	57	4	0	306	19	15
TO	0.2–0.3	855	677	0	0	0.08	4.08	0.06	0	0	6	44	6	0	229	17	11
TO	0.3–0.5	632	457	0	0	0.07	3.36	0	0	0	6	42	6	0	219	33	13
TO	0.5–1	574	438	4.6	0	0.07	3.39	0.07	0	0	4	40	8	0	171	15	13
TO	1–2	436	359	4.3	1	0.06	3.43	0.12	0	0	4	23	13	0	147	25	11
FE	0.063–0.2	1,064	59	1.8	0	5.53	0.53	0	0	0	0	15	6	0	6	44	21
FE	0.2–0.3	807	30	3.4	0	4.52	0.39	0	0	0	0	15	4	0	4	33	19
FE	0.3–0.5	741	42	7.7	0	2.95	0.36	0	0	0	0	16	2	0	6	33	14
FE	0.5–1	584	20	3.4	0	1.80	0.30	0	0	0	0	17	2	0	4	36	15
FE	1–2	528	18	6.4	0	1.45	0.32	0	0	0	0	15	2	0	11	29	13
FC	0.063–0.2	1,043	5	0	0	38.53	1.05	0	4	0	2	19	27	0	31	13	31
FC	0.2–0.3	919	15	4.6	0	37.32	0.89	0	2	0	2	17	15	0	27	13	20
FC	0.3–0.5	779	13	15.5	1	25.20	0.93	0	0	0	2	19	10	0	23	16	10

(Continued on following page)

TABLE 3 (Continued) Leaching test results for elements subject to regulation for plants (d.l.igs 156/2006). Red indicates concentrations exceeding legal limits.

Element	Cl ⁻	SO ₄ ²⁻	F ⁻	PO ₄ ³⁻	Ba	Cu	Zn	As	Be	Co	Ni	V	Cd	Cr	Pb	Se
Legal limit	100 mg/	250 mg/	1.5 mg/	2 mg/	1 mg/	0.05 mg/	3 mg/	50 ug/	10 ug/	250 ug/	10 ug/	250 ug/	5 ug/	50 ug/	50 ug/	10 ug/
WtE plant												ug/l				
Grain size (mm)				mg/l												
0.5-1	695	45	5.1	4	12.50	0.88	0	0	0	2	21	8	0	37	55	14
1-2	608	47	5.1	0	0.80	0.74	0	0	0	2	21	6	0	41	10	14

Zn and Mg are released only in the TO and PR plants, possibly in relation to ettringite dissolution. In TO, the leaching of SO₄, Co, Cu, Mg, and Zn is higher than that in other plants, and in PC, B and Mo show higher leaching. These differences, which are more than one order of magnitude, look specific to a WtE plant, or at least to the analyzed sampling from that plant.

Cu, Cr, and Ni are, among the PTEs, the most released in all plants with values below 0.5%, except for TO, where Cu stands at 3%. On the other hand, the release of Ti, Pb, and Zn is relatively low (<0.01%) and never exceeds law limits (Legislative Decree 152/06), suggesting their presence in a non-soluble structure, like glass or silicate minerals.

4 Conclusion

The bottom ashes from the WtE plants show an average composition remarkably similar in major elements, just with higher iron in TO and lower Si/higher LOI in PC. The chemical composition of major and minor elements changes with grain size, but within an order of magnitude and similarly in different plants. The similar BA composition could be related to a similar waste management approach in the area.

The mineralogy is different between HERA (FE and FC) and IREN (TO, PR, and PC) BA. In the former, we have lower amorphous and higher portlandite and ettringite, while in the latter, we do not have portlandite and the amorphous phases are between 60% and 90%. This affects leaching, which occurs in different basic environments: the leachates show higher sulfate and Al in IREN plants and lower sulfate and higher Ca in HERA plants. Leaching up to two orders of magnitude lower in Ba and Sr and higher in Cr occurs in IREN. The balance of Cl leaching shows that alkaline chlorides account for approximately 30%–35% of the global Cl, a fraction that does not show significant changes with grain size and between WtE plants, and is similar to the findings by Alam et al. (2020).

For most elements, composition and leaching are size-dependent but almost invariably within an order of magnitude. Some elements, such as Cl, Zn, S, and the LOI, decrease with grain size, but for other PTEs such as Ni, Cr, Co, and Pb, this is not a rule. Leaching increases in smaller grains for almost any element, but again within an order of magnitude, whereas between WtE plants, we find higher variability in leaching efficiency. From a circular economy perspective, reuse of BA as a supplementary material in concrete is possible: the presence of cement-related minerals such as portlandite in FE and FC supports reuse in the concrete, facilitating the setting and hardening reactions. However, significant concentrations of Cl and S, especially in the finer grain size, could be disadvantageous for cement application, and a pre-treatment before application as cement binding could be envisaged. Grain sorting could be useful in cases where the leaching of the larger grain size falls below the legislative limits of a given element, while the smaller grains do not, such as Cr in PC and Cu in PR. It could be more profitable to gain acquaintance with the mineralogical and chemical dissolution behavior of the BA from a given plant, as the differences in the leaching of minor elements look more dependent on the mineralogy than grain size.

Data availability statement

The original contributions presented in the study are included in the article/[Supplementary Material](#); further inquiries can be directed to the corresponding author.

Author contributions

LM and MT: conceptualization, methodology, data collection, data calculation, writing—original draft, and writing—review and editing. CD, PP, ED, ST, VF, and TB: methodology, data collection, data curation, and editing. LM, MT, CD, PP, ED, ST, VF, and TB have read and agreed to the published version of the manuscript. All authors contributed to the article and approved the submitted version.

Funding

This research was financially supported by the program “BANDO ATENEO per la ricerca 2021” of University of Parma and PRIN 2017 2017L83S77_005 “Mineral reactivity, a key to understand large-scale processes: from rock forming environments to solid waste recovering/lithification.” In addition, this work was benefited from the equipment and framework of the COMP-HUB Initiative, funded by the “Departments of Excellence” program of the Italian Ministry for Education, University and Research (MIUR 2018–2022).

References

- Alam, Q., Lazaro, A., Schollbach, K., and Brouwers, H. J. H. (2020). Chemical speciation, distribution and leaching behavior of chlorides from municipal solid waste incineration bottom ash. *Chemosphere* 241, 124985. doi:10.1016/j.chemosphere.2019.124985
- Alam, Q., Schollbach, K., van Hoek, C., van der Laan, S., de Wolf, T., and Brouwers, H. J. H. (2019). In-depth mineralogical quantification of MSWI bottom ash phases and their association with potentially toxic elements. *Waste Manag.* 87, 1–12. doi:10.1016/j.wasman.2019.01.031
- Astrup, T., Muntoni, A., Poletti, A., van Gerven, T., and van Zomeren, A. (2016). “Treatment and reuse of incineration bottom ash,” in *Environmental materials and waste* (Massachusetts, United States: Academic Press), 607–645.
- Bawab, J., Khatib, J., Kenai, S., and Sonebi, M. (2021). Buildings A review on cementitious materials including municipal solid waste incineration bottom ash (MSWI-BA) as aggregates. *Buildings* 11, 179. doi:10.3390/buildings11050179
- Bayuseno, A. P., and Schmahl, W. W. (2010). Understanding the chemical and mineralogical properties of the inorganic portion of MSWI bottom ash. *Waste Manag.* 30, 1509–1520. doi:10.1016/j.wasman.2010.03.010
- Caviglia, C., Confalonieri, G., Corazzari, I., Destefanis, E., Mandrone, G., Pastoro, L., et al. (2019). Effects of particle size on properties and thermal inertization of bottom ashes (MSW of Turin’s incinerator). *Waste Manag.* 84, 340–354. doi:10.1016/j.wasman.2018.11.050
- CEWEP (2016). Bottom ash fact sheet. Available at: <https://www.cewep.eu/bottom-ash-factsheet/> (Accessed October 20, 2021).
- Chimenos, J. M., Segarra, M., Fernández, M. A., and Espiell, F. (1999). Characterization of the bottom ash in municipal solid waste incinerator. *J. Hazard Mater* 64, 211–222. doi:10.1016/S0304-3894(98)00246-5
- EN 12457-4 (2004). *Waste characterization—leaching—compliance test for leaching of granular and sludge waste—Part 2: Single stage test, with a liquid/solid ratio of 10 L/kg, for materials with particles smaller than 4 mm (with or without size reduction)*. Available at: <https://store.uni.com/en/uni-en-12457-4-2004> (Accessed October, 2021).
- Criado, Y. A., Arias, B., and Abanades, J. C. (2018). Effect of the carbonation temperature on the CO₂ carrying capacity of CaO. doi:10.1021/acs.iecr.8b02111
- del Valle-Zermeño, R., Gómez-Manrique, J., Giro-Paloma, J., Formosa, J., and Chimenos, J. M. (2017). Material characterization of the MSWI bottom ash as a function of particle size. Effects of glass recycling over time. *Sci. Total Environ.* 581–582, 897–905. doi:10.1016/j.scitotenv.2017.01.047
- Dijkstra, J. J., Meeussen, J. C. L., and Comans, R. N. J. (2009). Evaluation of a generic multisurface sorption model for inorganic soil contaminants. *Environ. Sci. Technol.* 43, 6196–6201. doi:10.1021/es900555g
- Dou, X., Ren, F., Nguyen, M. Q., Ahamed, A., Yin, K., Chan, W. P., et al. (2017). Review of MSWI bottom ash utilization from perspectives of collective characterization, treatment and existing application. *Renew. Sustain. Energy Rev.* 79, 24–38. doi:10.1016/j.rser.2017.05.044
- Ente Nazionale Italiano di Unificazione (2020). Tests to determine the geometric characteristics of aggregates—Part 2: Determination of the particle size distribution—control sieves, nominal dimensions of the openings. *UNI En.* 933-2, 2020.
- Eusden, J. D., Eighmy, T. T., Hockert, K., Holland, E., and Marsella, K. (1999). Petrogenesis of municipal solid waste combustion bottom ash. *Appl. Geochem.* 14, 1073–1091. doi:10.1016/S0883-2927(99)00005-0
- Frantini, M., Leoni, L., and Saitta, M. (1972). A simple method to evaluate the matrix effects in X-Ray fluorescence analysis. *X-Ray Spectrom.* 1, 151–154. doi:10.1002/xrs.1300010406
- Fridrichová, M., Dvolák, K., Gazdii, D., Mokrá, J., and Kulisek, K. (2016). Thermodynamic stability of ettringite formed by hydration of ye’elime clinker. *Adv. Mater. Sci. Eng.* 2016, 9280131. doi:10.1155/2016/9280131
- Fuller, W. B., and Thompson, S. E. (1907). The laws of proportioning concrete. *Trans. Am. Soc. Civ. Eng.* 59, 67–143. doi:10.1061/TACEAT.0001979
- Funari, V., Braga, R., Bokhari, S. N. H., Dinelli, E., and Meisel, T. (2015). Solid residues from Italian municipal solid waste incinerators: A source for “critical” raw materials. *Waste Manag.* 45, 206–216. doi:10.1016/j.wasman.2014.11.005
- Ginés, O., Chimenos, J. M., Vizcarro, A., Formosa, J., and Rosell, J. R. (2009). Combined use of MSWI bottom ash and fly ash as aggregate in concrete formulation: Environmental and mechanical considerations. *J. Hazard Mater* 169, 643–650. doi:10.1016/j.jhazmat.2009.03.141

Acknowledgments

The authors would like to thank Andrea Comelli, Luca Barchi, and Roberta Magnani for their help during samplings (thin-section preparation, SEM analysis, and TGA).

Conflict of interest

The authors declare that the research was conducted in the absence of any commercial or financial relationships that could be construed as a potential conflict of interest.

The handling editor MCD declared a past collaboration with the author MT.

Publisher’s note

All claims expressed in this article are solely those of the authors and do not necessarily represent those of their affiliated organizations, or those of the publisher, the editors, and the reviewers. Any product that may be evaluated in this article, or claim that may be made by its manufacturer, is not guaranteed or endorsed by the publisher.

Supplementary material

The Supplementary Material for this article can be found online at: <https://www.frontiersin.org/articles/10.3389/fenvs.2023.1179272/full#supplementary-material>

- Heiri, O., Lotter, A. F., and Lemcke, G. (2001). Loss on ignition as a method for estimating organic and carbonate content in sediments: Reproducibility and comparability of results. *J. Paleolimnol.* 25, 101–110. doi:10.1023/A:1008119611481
- Hera Ambiente, S. p. A. (2020). *Dichiarazione ambientale complesso impiantistico forli'*. Available at: <http://ha.gruppohera.it> (Accessed October, 2021).
- Huber, F., Blasenbauer, D., Aschenbrenner, P., and Fellner, J. (2020). Complete determination of the material composition of municipal solid waste incineration bottom ash. *Waste Manag.* 102, 677–685. doi:10.1016/j.wasman.2019.11.036
- Hyks, J., Verginelli, I., Costa, G., Hjelm, O., and Lombardi, F. (2018). Leaching behaviour of incineration bottom ash in a reuse scenario: 12 years-Field data vs. lab test results. *Waste Manag.* 73, 367–380. doi:10.1016/J.WASMAN.2017.08.013
- Iren Ambiente, S. (2018). *Dichiarazione Ambientale 2018 relativa al sito: Impianto di Termovalorizzazione di Piacenza*. Available at: www.gruppoiren.it (Accessed October, 2021).
- Itto, R., Fujita, T., Sadaki, J., Matsumoto, Y., and Ahn, J.-W. (2006). Removal of chloride in bottom ash from the industrial and municipal solid waste incinerators. *Int. J. Soc. Mater. Eng. Resour.* 13, 70–74. doi:10.5188/ijmsr.13.70
- Izquierdo, M., López-Soler, Á., Vazquez Ramonich, E., Barra, M., and Querol, X. (2002). Characterisation of bottom ash from municipal solid waste incineration in Catalonia. *J. Chem. Technol. Biotechnol.* 77, 576–583. doi:10.1002/jctb.605
- Karamanov, A., Karamanova, E., Schabbach, L. M., Andreola, F., Taurino, R., and Barbieri, L. (2021). Sintering and phase formation of ceramics based on pre-treated municipal incinerator bottom ash. *Open Ceram.* 5, 100044. doi:10.1016/j.oceram.2020.100044
- Kaza, S., Yao, L. C., Bhada-Tata, P., and Woerde, F. V. (2018). *What a waste 2.0: A global snapshot of solid waste management to 2050*. NW, Washington, D.C.: The World Bank Publication.
- Kleib, J., Aouad, G., Abriak, N. E., and Benzerzour, M. (2021). Production of portland cement clinker from French municipal solid waste incineration bottom ash. *Case Stud. Constr. Mater.* 15, e00629. doi:10.1016/j.cscm.2021.e00629
- Loginova, E., Volkov, D. S., van de Wouw, P. M. F., Florea, M. V. A., and Brouwers, H. J. H. (2019). Detailed characterization of particle size fractions of municipal solid waste incineration bottom ash. *J. Clean. Prod.* 207, 866–874. doi:10.1016/j.jclepro.2018.10.022
- Mantovani, L., Tribaudino, M., Matteis, C., and Funari, V. (2021). Particle size and potential toxic element speciation in municipal solid waste incineration (MSWI) bottom ash. *Sustainability* 13, 1911. doi:10.3390/su13041911
- Meima, J. A., and Comans, R. N. J. (1999). The leaching of trace elements from municipal solid waste incinerator bottom ash at different stages of weathering. *Appl. Geochem.* 14, 159–171. doi:10.1016/S0883-2927(98)00047-X
- Menéndez, E., Andrade, C., and Vega, L. (2012). Study of dehydration and rehydration processes of portlandite in mature and young cement pastes. *J. Therm. Anal. Calorim.* 110, 443–450. doi:10.1007/s10973-011-2167-4
- Piantone, P., Bodéan, F., and Chatelet-Snidaro, L. (2004). Mineralogical study of secondary mineral phases from weathered MSWI bottom ash: Implications for the modelling and trapping of heavy metals. *Appl. Geochem.* 19, 1891–1904. doi:10.1016/j.apgeochem.2004.05.006
- Rungchet, A., Poon, C. S., Chindaprasirt, P., and Pimraksa, K. (2017). Synthesis of low-temperature calcium sulfoaluminate-belite cements from industrial wastes and their hydration: Comparative studies between lignite fly ash and bottom ash. *Cem. Concr. Compos.* 83, 10–19. doi:10.1016/j.cemconcomp.2017.06.013
- Setoodeh Jahromy, S., Jordan, C., Azam, M., Werner, A., Harasek, M., and Winter, F. (2019). Fly ash from municipal solid waste incineration as a potential thermochemical energy storage material. *Energy Fuels* 33, 5810–5819. doi:10.1021/acs.energyfuels.8b04106
- Suárez-Macias, J., María Terrones-Saeta, J., Javier Iglesias-Godino, F., Antonio Corpas-Iglesias, F., Rubio-Gámez, M., and Jiménez del Barco Carrión, A. (2021). Evaluation of physical, chemical, and environmental properties of biomass bottom ash for use as a filler in bituminous mixtures. *Sustainability* 13, 4119. doi:10.3390/su13084119
- Šyc, M., Krausová, A., Kameníková, P., Šomplák, R., Pavlas, M., Zach, B., et al. (2018). Material analysis of Bottom ash from waste-to-energy plants. *Waste Manag.* 73, 360–366. doi:10.1016/j.wasman.2017.10.045
- Šyc, M., Simon, F. G., Hyks, J., Braga, R., Biganzoli, L., Costa, G., et al. (2020). Metal recovery from incineration bottom ash: State-of-the-art and recent developments. *J. Hazard Mater* 393, 122433. doi:10.1016/j.jhazmat.2020.122433
- Toby, B. H., and von Dreele, R. B. (2013). *GSAS-II: The Genesis of a modern open-source all purpose crystallography software package*. *J. Appl. Crystallogr.* 46, 544–549. doi:10.1107/S0021889813003531
- Toller, S., Funari, V., Vasumini, I., and Dinelli, E. (2021). Geochemical characterization of surface sediments from the Ridracoli reservoir area and surroundings, Italy. Details on bulk composition and grain size. *J. Geochem Explor* 231, 106863. doi:10.1016/J.GEXPLO.2021.106863
- Trifunovic, P. D., Marinkovic, S. R., Tokalic, R. D., and Matijasevic, S. D. (2010). The effect of the content of unburned carbon in bottom ash on its applicability for road construction. *Thermochim. Acta* 498, 1–6. doi:10.1016/j.tca.2009.10.022
- Wei, Y., Shimaoka, T., Saffarzadeh, A., and Takahashi, F. (2011a). Alteration of municipal solid waste incineration bottom ash focusing on the evolution of iron-rich constituents. *Waste Manag.* 31, 1992–2000. doi:10.1016/j.wasman.2011.04.021
- Wei, Y., Shimaoka, T., Saffarzadeh, A., and Takahashi, F. (2011b). Mineralogical characterization of municipal solid waste incineration bottom ash with an emphasis on heavy metal-bearing phases. *J. Hazard Mater* 187, 534–543. doi:10.1016/j.jhazmat.2011.01.070
- Winnefeld, F., and Lothenbach, B. (2010). Hydration of calcium sulfoaluminate cements - experimental findings and thermodynamic modelling. *Cem. Concr. Res.* 40, 1239–1247. doi:10.1016/j.cemconres.2009.08.014
- Yadav, V. K., Gacem, A., Choudhary, N., Rai, A., Kumar, P., Yadav, K. K., et al. (2022). Status of coal-based thermal power plants, coal fly ash production, utilization in India and their emerging applications. *Minerals* 12, 1503. doi:10.3390/min12121503
- Zanelli, C., Conte, S., Molinari, C., Soldati, R., and Dondi, M. (2021). Waste recycling in ceramic tiles: A technological outlook. *Resour. Conserv. Recycl.* 168, 105289. doi:10.1016/j.resconrec.2020.105289
- Zevenbergen, C., van Reeuwijk, L. P., Bradley, J. P., Comans, R. N. J., and Schuiling, R. D. (1998). Weathering of MSWI bottom ash with emphasis on the glassy constituents. *J. Geochem Explor* 62, 293–298. doi:10.1016/S0375-6742(97)00033-2